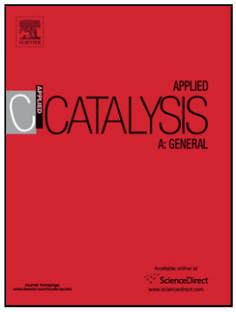

Title: $BaTi1_{-x}Cu_xO_3$ perovskites: The effect of copper content in the properties and in the NOx storage capacity

Author: Vicente Albaladejo-Fuentes Franz Edwin López-Suárez María Salvadora Sánchez-Adsuar María José Illán-Gómez

PII: S0926-860X(14)00583-3
DOI: http://dx.doi.org/doi:10.1016/j.apcata.2014.09.032
Reference: APCATA 15013

To appear in: *Applied Catalysis A: General*

Received date: 4-7-2014
Revised date: 1-9-2014
Accepted date: 21-9-2014

Please cite this article as: V. Albaladejo-Fuentes, F.E. López-Suárez, M.S. Sánchez-Adsuar, M.J. Illán-Gómez, $_{-x}Cu_xO_3$ perovskites: the effect of copper content in the properties and in the NOx storage capacity., *Applied Catalysis A, General* (2014), http://dx.doi.org/10.1016/j.apcata.2014.09.032

$_{-x}Cu_xO_3$ perovskites: the effect of copper content in the properties and in the NOx storage capacity.

Vicente Albaladejo-Fuentes[a], Franz Edwin López-Suárez[b], María Salvadora Sánchez-Adsuar[a], María José Illán-Gómez[a]

[a]*Carbon Materials and Environment Research Group, Department of Inorganic Chemistry, Faculty of Science, Universidad de Alicante, Alicante, Spain*

[b] *Instituto de Tecnologia e Pesquisa, Universidade Tirandentes, Aracaju – Sergipe, Brasil.*

Research Highlights

- The incorporation of copper into the lattice distorts the perovskite structure.
- $BaTi_{1-x}Cu_xO_3$ catalysts are active for NO to NO_2 oxidation and for NOx adsorption.
- NOx storage capacity of the $BaTi_{1-x}Cu_xO_3$ catalysts increases with copper content.
- BaTiCu2 shows a NOx storage capacity close to noble metal-based catalysts.

Abstract

$BaTi_{1-x}Cu_xO_3$ perovskites have been prepared by the Pechini's sol-gel method and the effect of copper in the structural and physico-chemical properties of the perovskites and in the performance of the catalysts for NOx storage has been studied.

XRD and Raman spectroscopy results indicate that all the copper containing catalysts present a distortion of the original tetragonal structure due to the incorporation of copper into the lattice. The XPS and H_2-TPR results reveal that the copper catalysts, except for BaTiCu0.5 catalyst, present two copper species (with different electronic interaction with the perovskite) and active surface oxygen species. Additionally, it seems that the fraction of copper with a strong electronic interaction with the perovskite or incorporated into the perovskite structure increases with the copper content.

The active sites created on the $BaTi_{1-x}Cu_xO_3$ perovskite surface bring to the catalysts activity for the NO to NO_2 oxidation and for the NOx adsorption. The NOx storage capacity increases with the copper content and reaches a limit for the BaTiCu2 catalyst (300 μmol/g, at 420ºC) which is within the range of the values reported for the noble metal-based catalysts.

Keywords

Perovskite, NOx storage, copper, sol-gel method, NO to NO_2 oxidation

Graphical Abstract

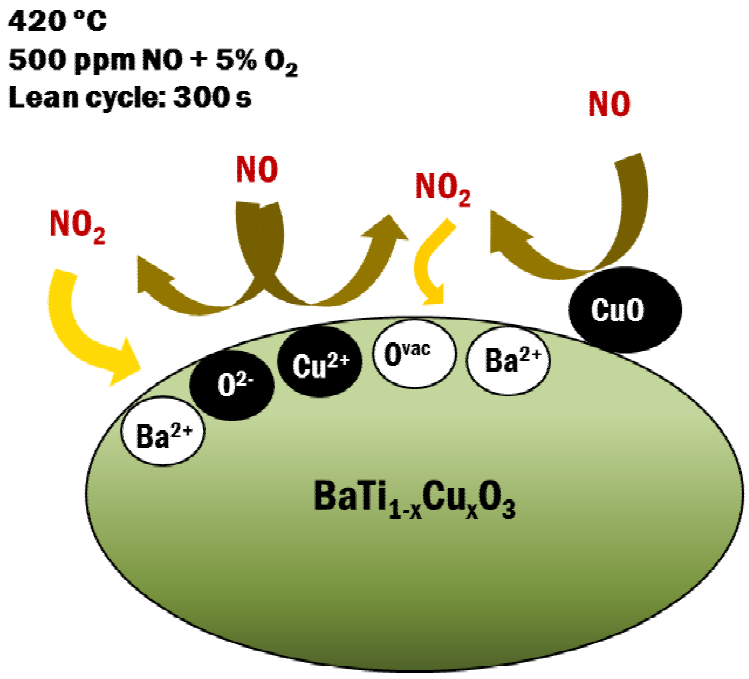

I. Introduction

The main pollutants emitted by diesel engines are nitrogen oxides (NOx) and soot particles. Due to their adverse effects on the environment and human health, the concentration of these pollutants is limited by legislation. In order to meet the current and upcoming Emission Standard Legislation (Euro VI (2014) regulations in Europe), the removal of NOx and soot from diesel exhaust is a research issue of great interest [1, 2]. Currently, Diesel Particulate Filters (DPF) [3] are used for soot control in diesel exhaust but, the NOx control is still unresolved because the three-way technology, used on gasoline-powered engines, is unable to reduce NOx under the usual lean conditions of diesel engines and lean burn gasoline engines. There are three alternatives for NOx conversion into innocuous gases [4]: (i) direct decomposition, (ii) selective

catalytic reduction (SCR), and (iii) NOx Storage and Reduction (NSR), also known as Lean NOx Trap (LNT) [5, 6]. The direct decomposition of NO is thermodynamically favorable, but the high activation energy of the reaction limits the practical use of this approach. SCR is based on the NOx reduction using H_2, hydrocarbons, NH_3 or urea in the presence of a selective catalyst able to promote the NOx reduction reaction in an oxygen rich environment [1, 7, 8]. NSR, which is the approach used in this study, works under cyclic conditions: i) under lean conditions, when oxygen is in excess, NOx is adsorbed on the catalyst, and ii) under rich conditions, achieved by adding a reductant, the NOx reduction takes place [9]. A typical NSR catalyst, as that proposed by Toyota, is based in a high surface area support material (often γ–alumina), a NOx storage material (Ba or K) [9] and a noble metal able to catalyze the NO oxidation to NO_2, under lean conditions and, also the reduction of the stored NOx, under rich conditions [1, 4]. The most efficient catalysts used for NSR are based in platinum supported on mixed oxides or zeolites. However, this composition presents certain limitations, such as: *i)* reduction of the NOx storage capacity at temperature above 450°C, *ii)* low thermal stability, *iii)* catalyst poisoning by formation of barium carbonates and sulfates [10-14] and iv) unsatisfactory efficiency for certain applications, such as lean burn gasoline engines (GDI, gasoline direct injection), with exhaust temperatures as high as 400-500ºC [15]. Nowadays, an intense research is being carried out in order to propose alternatives to the use of noble metal-based catalysts for NSR able to work even at high temperatures (400-500ºC) [16].

The $BaTiO_3$ mixed oxides, with perovskite structure, are being widely used as multilayer capacitors (MLC), sonar and ultrasonic transducers, positive temperature coefficient (PTC) heaters, sensors, and ferroelectric thin-film memories [17-21] due to its ferroelectrics, dielectrics, piezoelectrics and pyroelectrics properties [18, 21, 22].

The perovskites are mixed oxides with ABO_3 stoichiometry with an ideal structure which must keep the relation $r_A + r_o = \sqrt{2}(r_B + r_o)$ [23]. Interestingly, a lot of multi-components mixed oxides can be obtained by partial substitution of A and B cations. This substitution does not cause a change in the structure but it generates a modification of the physico-chemical properties of the raw mixed oxides. The tolerance factor, *t,* introduced by *Goldschmidt* [24], $t = r_A + r_o / \sqrt{2}(r_B + r_o)$, is being used for measuring the degree of distortion generated by the substitution process. The *t* values for perovskites are between 0.75 and 1 (for an ideal structure). Partial substitution of cations could produce a non-stoichiometric perovskite with cationic and/or oxygen vacancies to fulfill the conditions of electro-neutrality of the solid [25]. The partial substitution of cations without affecting the perovskite structure has increased the interest of using these mixed oxides as catalysts. Additionally, perovskites are cheap and present a high thermal resistance; so, since the seventies, perovskites are being used also as catalysts.

Looking for alternatives for current platinum-based NSR catalysts, mixed oxides with perovskite structure have been recently used for NOx storage and reduction [26-36]. Thus, Ueda et al. [30] employed a $(La_{0.7}Ba_{0.3})(Fe_{0.776}Nb_{0.194}Pd_{0.03})O_3$ perovskite as an effective NSR catalyst. Hodjati et al. [29] analysed the NOx adsorption-desorption processes on ABO_3 perovskites, with A = Ca, Sr, or Ba and B = Sn, Zr, or Ti, and they concluded that for A sites, the activity order is Ba >Sr>Ca and, for B sites, it is Sn>Zr> Ti. Kim et al. [31] showed that lanthanum perovskites ($La_{1-x}Sr_xCoO_3$) present a NO to NO_2 oxidation behavior close to platinum based catalysts. Also, Li et al. [34] demonstrated that these lanthanum based perovskites exhibit a high NOx conversion and N_2 selectivity for different gas composition. Furthermore, it was proved that the incorporation of Fe into the perovskite structure improves the sulfur tolerance of the catalysts [35, 36]. In previous papers [32, 33], the authors concluded that the incorporation of copper into the structure

of $SrTiO_3$ perovskites ($SrTi_{1-x}Cu_xO_3$) produces catalysts with a high capacity for the NO oxidation to NO_2 and for the NOx storage.

Considering that Ba [29] presents a higher NOx adsorption capacity than Sr and the role of Cu previously indicated [32, 33] the aim of this study is to determine the effect of copper in the structural and physico-chemical properties of a $BaTiO_3$ perovskite, as well as to test the performance for the NOx storage of four copper perovskite catalysts with different copper content ($BaTi_{1-x}Cu_xO_3$).

II. Experimental

Catalysts preparation

$BaTi_{1-x}Cu_xO_3$ catalysts (x = 0.05, 0.1, 0.2 and 0.3) were prepared using the Pechini's sol-gel method [37] modified to be used in an aqueous media [38-40]. Titanium isopropoxide, barium acetate and copper nitrate were used as precursors. In brief, the titanium isopropoxide (Ti) was hydrolyzed and the resulting species was dissolved in an aqueous solution of citric acid (CA) (Ti:CA = 1:2) and hydrogen peroxide ($Ti:H_2O_2$ = 2:1), forming the citrate-peroxo-titanate (IV) complex. Afterwards, the pH was adjusted to 8.5 with NH_3, and barium (Ba:Ti = 1:1) and copper precursor were added using the amount corresponding to the stoichiometry ($BaTi_{1-x}Cu_xO_3$). The solution was kept at 65ºC for 5h, until a gel was obtained, which was later dried at 90ºC for 24h and, finally, calcined at 850ºC for 6h.

Catalysts characterization

The copper content of catalysts was measured by ICP-OES in a Perkin–Elmer device, model Optimal 4300 DV. For this purpose, the metal was extracted from catalysts by refluxing them in 8M HCl solution for 2h.

The BET surface areas were determined by physical adsorption of N_2 at –196ºC in an automatic volumetric system (Autosorb-6B from Quantachrome) after degassing the samples at 250ºC for 4h.

The crystalline structure was obtained by XRD and Raman spectroscopy. X-ray diffractograms were recorded in a Seifert powder diffractometer, using CuKα (0,15418 nm) radiation. Diffractograms were registered between 2θ angles from 20 to 80º, with a step of 0.02º and a time per step of 3 seconds. Raman spectra were obtained using a Bruker RFS 100/S Fourier Transform Raman Spectrometer with a variable power Nd:YAG laser source (785 nm).

XPS were obtained using a K-Alpha Photoelectron Spectrometer by Thermo-Scientific with an Al Kα (1486.7 eV) radiation source. To obtain XPS spectra, the pressure of the analysis chamber was maintained at $5 \cdot 10^{-10}$ mbar. The binding energy (BE) and kinetic energy (KE) scales were adjusted by setting the C 1s transition at 284.6 eV, and the BE and KE values were then determined with the peak-fit software of the spectrometer.

Temperature Programmed Reduction experiments with H_2 (H_2-TPR) and Temperature Programmed Desorption (TPD) were carried out in a Micromeritics device (model Pulse ChemiSorb 2705). The sample was heated at 10ºC/min from 25 to 900ºC under a 5% H_2/Ar flow (40 ml/min, Ptotal = 1 atm) for the H_2-TPR experiments and under a He flow (40 ml/min, Ptotal

= 1 atm) for the TPD experiments. A TCD detector was used to determine the outlet gas composition. A CuO reference sample supplied by Micromeritics was used to quantify H_2 consumption.

NOx storage tests

NOx storage tests were performed in a fixed-bed reactor at atmospheric pressure under a gas flow (500 ml/min) containing 500 ppm NO, 5 % O_2 in N_2 balance. The catalytic bed was composed by 80 mg of catalyst and 320 mg of SiC. The gas composition was monitored by specific NDIR-UV gas analysers for NO, NO_2, CO, CO_2 and O_2 (Rosemount Analytical Model BINOS 1001, 1004 and 100). Temperature programmed reactions (10ºC/min from room temperature to 800ºC) were performed using the as-prepared catalyst. NOx conversion profiles were determined as a function of temperature using the following equation:

$$\text{NOx conversion } (\%) = \frac{NOx_{in} - NOx_{out}}{NOx_{in}} \times 100 \qquad (1)$$

where "NOx_{in}" is the concentration of NOx (= NO+NO_2) fed to the reactor, "NOx_{out}" and "NO_{2out}", are the concentration of NOx and NO_2 which left the reactor.

The percentage of NO_2 generated during temperature programmed reactions was calculated by using:

$$NO_2(\%) = \frac{NO_{2out}}{NOx_{out}} \times 100 \qquad (2)$$

For isothermal experiments consecutive NOx storage-reduction cycles were carried out, at the selected temperature, using the same batch of sample and a gas flow of 500 ml/min (GHSV 30000h^{-1}). The NOx storage capacity was determined by carrying out ten consecutives storage – reduction cycles, using the following procedure: i) during the rich cycle (3 minutes), a rich gas flow (10% H_2 as model reductant in N_2 balance) was fed through the reactor while a lean gas flow (500 ppm NO + 5% O_2 in N_2 balance) was fed, by a bypass path, through the gas analysers, ii) at the required time, the gas paths were changed and during the lean cycle (5 minutes), the lean gas flow was fed through the reactor and, subsequently, to the gas analysers. This procedure was also carried out using a reactor without catalyst (400 mg of SiC) to determine the $NOx_{,inlet}$ response of the gas analysers. Note that, even the time of rich and lean cycles is far from that of the realistic conditions, it is convenient to determine the ability of catalysts for NOx storage.

The NOx storage capacity was calculated as the difference between the NOx signal when the reactor is empty and the NOx signal when the reactor is filled with a catalyst, by using:

$$\text{NOx storage} = \int_{t_0}^{t_f} NO_{x,inlet}(t) - NO_{x,\exp}(t)dt \qquad (3)$$

where "NOx_{inlet}" is the concentration of NOx (= NO+NO_2) measured for the empty reactor, and "$NO_{x,exp}$", is the concentration of NOx during the NOx storage test.

III. Results and discussion

Textural and structural characterization

The copper content (measured by ICP-OES) and the BET surface area (obtained from N_2 adsorption isotherm) for $BaTi_{1-x}Cu_xO_3$ catalysts with different copper content (x= 0, 0.05, 0.1, 0.2, 0.3) are included in Table 1.

The ICP-OES results reveal, as expected, that all the copper added during synthesis process is present in the catalysts. The N_2 adsorption isotherms and the BET surface areas obtained for the catalysts, and calculated from the isotherm data by applying the BET equation [41], are the corresponding to solids with negligible porosity, as mixed oxides with perovskite structure are [23, 32]. However, the BET surface areas show a slight increase with the copper content as consequence of the creation of oxygen vacancies on the catalyst structure, due to the presence of copper into the lattice as it will be discussed below.

Figures 1a and 1b show the XRD patterns of catalysts including the corresponding to a commercial $BaTiO_3$ (Sigma-Aldrich) used as reference material (BaTiref). All the XRD patterns show the main peaks corresponding to the tetragonal $BaTiO_3$ perovskite at 2θ: 22,3º; 31,4º; 38,8º; 45,2º; 51,0 º; 56,1º; 65,8º; 74,9º; for (100), (110), (111), (200), (210), (211), (220) and (310) lattice planes, respectively [42].

For copper-perovskites $BaCO_3$ and Ba_2TiO_4 are also identified as segregated phases. The $BaCO_3$ is formed by the carbonation of segregated barium oxide during samples atmospheric exposure. Note that the intensity of the corresponding peaks increases with the copper content.

In addition, for high copper content BaTiCu2 and BaTiCu3 catalysts, the presence of CuO and TiO_2 (rutile) [43] as segregated phases are also identified. This indicates that only a fraction of Cu loaded was incorporated into the perovskite structure. Also, a decrease in the intensity of the perovskite main peak (110) and a shift to a higher diffraction angle are observed for BaTiCu2 and BaTiCu3 catalysts (Figure 1b). On the contrary, for low copper content BaTiCu0.5 and BaTiCu1 catalysts, peaks corresponding to CuO and TiO_2 (rutile) are not clearly observed, so, it means that these phases are not segregated or, if they are, they present a crystallite size under the detection limit of XRD technique.

The average crystal size for all catalyst, including the commercial $BaTiO_3$, was calculated from the Full Width at Half Maximum (FWHM) of the (110) peak by using the Scherrer equation and the data are also included in Table 1 [44]. Identical average crystal sizes are obtained for bare perovskites BaTi and BaTiref (29 nm) while, for copper catalysts, the average crystal size is larger, ranging from 35 nm to 38 nm.

Hakuta et al. [42, 45] proposed that by comparing the FWHM of (200) and (111) XRD peaks (Figure 1b), it is possible to determine if a perovskite presents a cubic or a tetragonal structure. Thus, if FWHM of (200) peak is larger than FWHM of (111) peak, it can be established that the perovskite presents a tetragonal structure. Table 1 shows that the FWHM (200) / (111) ratio is higher than 1 for all samples and, consequently, it can be concluded that the synthesis method produces perovskites with tetragonal structure. Using Difracc plus software ®, and the position of the (110) and (111) peaks (Figure 1b), the lattice parameters *a* and *c* corresponding to tetragonal structure were calculated and the data are also featured in Table 1. These parameters, and mainly the parameter *a*, are different for $BaTi_{1-x}Cu_xO_3$ catalysts. Thus, even though a clear

relationship with the copper content is not observed, these data suggest a distortion of the tetragonal structure due to copper incorporation into the perovskite structure.

The tetragonal structure of $BaTi_{1-x}Cu_xO_3$ catalysts has been verified by Raman spectroscopy and the spectra are shown in Figure 2. According to literature [46-48], the $BaTiO_3$ perovskite presents a tetragonal structure between 5ºC and 120ºC, and a cubic structure at temperature above 120ºC. The cubic structure belongs to space group *Pm3m* which does not present first-order Raman-active modes and, consequently, their spectra do not show any band. However, the tetragonal structure belongs to space group *P4mm* and it presents bands at, approximately, 180 cm^{-1}, 265 cm^{-1}, 305 cm^{-1}, 520 cm^{-1} and 720 cm^{-1} corresponding to irreducible representations (A1(LO)), (A1(TO)), (B1), (A1, E(TO)) and (A1, E(LO), respectively [47, 49]. The band located at 305 cm^{-1} is the most often used to differentiate between the cubic and tetragonal structure by Raman spectroscopy because this peak disappears when the tetragonal structure is not the main one. The Raman spectra of Figure 2 indicate that bare perovskites (BaTi and BaTiref) present a tetragonal structure. The incorporation of copper, as it was previously shown by XRD data, causes a distortion of the tetragonal structure which leads to a dramatic peaks broadening in the Raman spectra even though they do not disappear. In addition, the Raman spectra for $BaTi_{1-x}Cu_xO_3$ catalysts present a new band at ca. 750 cm^{-1} corresponding to a Ba_2TiO_4 phase, which is fairly observed for BaTiCu3 and BaTiCu2 [50, 51]. This founding agrees with XRD results and confirms that the copper incorporation causes the segregation of phases in the catalysts.

Therefore, from Raman spectroscopy and XRD data, it can be concluded that copper produces a distorsion of the tetragonal perovskite structure and generates the segregation of $BaCO_3$, TiO_2, Ba_2TiO_4 and CuO phases, mainly for high copper content BaTiCu2 and BaTiCu3 catalysts.

XPS characterization

XPS analysis provides additional information about the surface composition of the $BaTi_{1-x}Cu_xO_3$ perovskite catalysts. The XPS profiles corresponding to the Cu $2p^{3/2}$ transition and O1s transition, shown in Figure 3a and 3b respectively, offer information about the copper and oxygen species present on the catalyst surface.

Reduced copper species, such as metallic copper or Cu_2O, usually appear at binding energy (BE) close to 933 eV but, for Cu(II) species, the Cu $2p^{3/2}$ transition appears above 933 eV [33, 52-54]. In Figure 3a, it is observed that the BE maximum of the main XPS band appears above 933 eV for all copper catalysts, suggesting the presence of Cu(II) species. Cu(I) and Cu(II) species can be distinguished by the presence of a satellite peak at 942-945 eV due to an electron transfer from $Cu2p^{3/2}$ to 3d free level of Cu(II) [52]. All the copper catalysts show the satellite peak which indicates, also, the presence of Cu(II) species.

The deconvolution of the normalized Cu $2p^{3/2}$ bands reveals two contributions with maxima at 933.5±0.4 eV and 935.5±0.2 eV which seem to correspond to two different Cu (II) species: *i)* the band at lower BE, assignable to copper species with a weak electronic interation with the perovskite, that is, to CuO species located on the surface (Cu_S) and, *ii)* the band at higher BE, corresponding to copper species with a strong electronic interaction with the perovskite (Cu_L) [55]. Table 2 features some relevant data obtained from XPS results. It is observed that the percentage corresponding to the area of the XPS band at 935.5±0.2 eV (Cu_L band) increases with the copper content (from 43% to 53%), suggesting that the presence of copper with a strong electronic interaction with the perovskite is favoured as copper content increases. In fact, BaTiCu0.5 catalyst does not show the presence of Cu_L, while the percentage increases with the

copper content for the other three catalysts. Additionally, by comparing the Cu/Cu+Ti+Ba ratio calculated by XPS with the corresponding nominal ratio, it is deduced that copper has to be incorporated into the catalyst structure, since the XPS ratio and the nominal ratio are similar. (For BaTiCu2 XPS ratio is even lower than the nominal ratio.) On the other hand, the Cu+Ti/Ba ratio values (Table 2) are close to 0.5, which is far from 1, the value for the $BaTiO_3$ reference catalyst, and similar to the expected value for a Ba_2TiO_4 mixed oxide. On the contrary, the bare BaTi perovskite shows a Cu+Ti/Ba ratio similar to the obtained for the $BaTiO_3$ reference catalyst (BaTiref). These XPS results, in agreement with the XRD and Raman results, suggest that the addition of copper promotes the formation of Ba_2TiO_4 on the catalysts surface.

Figure 3b shows the XPS spectra of the O1s transition for all catalysts which are similar to those reported for other mixed oxides as $Ce_xLa_{1-x}O_2$ (x = 25, 50 or 75) [56], $SrTiCuO_3$ perovskites [33] and $La_{1-x}Sr_xMO_3$ (M = $Co_{0.77}Bi_{0.20}Pd_{0.03}$; $0 \leq x \leq 0.8$) [57]. After the bands deconvolution, three contributions at approximately 530 eV, 532 eV and 534 eV are identified: i) the O 1s band at ca. 530 eV corresponds to lattice oxygen of metal oxides (O_L) [58], ii) the band at ca. 532 eV has been assigned to adsorbed oxygen species, O_2^{2-}, surface carbonates, CO_3^{2-}, and/or hydroxyl groups, OH^-, (O*) and iii) the band at ca. 534 eV is associated with adsorbed water (H_2O) [56-59]. The intensity of these bands notably changes for copper perovskites, thus, the band at the lowest BE (O_L) decreases and the bands at higher BE (O* and H_2O) increase with copper content. In Table 3 it is observed that the percentage corresponding to the area of the O* band is larger for copper perovskites (around 50%) than for bare perovskites (around 35%). This seems to indicate the presence of a larger amount of oxygen surface species - such as O_2^{2-} species, OH^- groups, and/or carbonates - on copper perovskites. These oxygen surface species have been formed on the oxygen vacancies created on the perovskite surface after copper incorporation.

From XRD and Raman spectroscopy data it is concluded that the incorporation of copper into perovskite lattice produces a distortion of the tetragonal structure of the catalysts. Furthermore, the substitution of Ti^{4+} by Cu^{2+}cations causes a positive charge deficiency that could be compensated by the formation of oxygen vacancies [23] where oxygen surface species could be formed. Also, the presence of some Ti^{3+} species has been suggested as other possibility to stabilize the high oxygen vacancies level. In spite of this, the XPS profiles corresponding to the Ti 2*p* show only one peak at ca. 458 eV, which indicates that Ti^{4+}cations is the unique titanium oxidation state [60] and therefore, the presence of Ti^{3+}cations can be ruled out. Thus, the electroneutrality of the perovskite after the copper incorporation into the structure has to be achieved by the creation of oxygen vacancies, that is, by forming a non-stoichiometric perovskite ($BaTi_{1-x}Cu_xO_{3-\lambda}$). The O_L/Cu+Ti+Ba ratio (see Table 3), calculated from the peak area of $O1s_L$ (lattice oxygen), $Ti2p^{3/2}$, $Ba3d^{3/2}$ and $Cu2p^{3/2}$ transitions, is lower than that obtained for the BaTiref. This fact reveals that the introduction of copper into the perovskite lattice causes the generation of oxygen vacancies on the perovskite structure. Thus, even it is not possible to establish a correlation between the copper content and the O_L/Cu+Ti+Ba ratio, all the values are lower for the copper perovskites.

H_2- TPR characterization.

The redox properties of $BaTi_{1-x}Cu_xO_3$ catalysts have been determined by Temperature Programmed Reduction with hydrogen (H_2-TPR) and the H_2 consumption profiles are included in Figure 4. The H_2 consumption observed between 250 and 500ºC for all copper catalysts corresponds to the reduction of copper species since almost null H_2 consumption is shown by bare perovskite BaTi in this range of temperature. The molar percentage of reduced copper,

which is included in Table 1, increases with the copper content and this indicates that the reducibility of the catalysts is also improved with the percentage of copper. Most of the H_2 consumption profiles shown in Figure 4 present two quite well-defined peaks between 280 and 450 ºC which indicate the presence of two copper species with different reducibility. For the lowest copper content catalyst (BaTiCu0.5), only a very low intensity peak is observed around 400ºC, however, as the copper content increases, a quite well-defined peak appears at lower temperature (around 300ºC) which intensity increases with the copper content. These copper species with different reducibility have to correspond with copper species with different electronic interaction with the perovskite detected by XPS.

The peak appearing at 400ºC for the lowest copper content catalyst (BaTiCu0.5) could be attributed to surface copper species with a weak electronic interaction with the perovskite, as its reducibility is similar to that of the CuO used as reference. As copper content increases, this peak becomes a shoulder of the higher intensity peak appearing at lower temperature (300ºC) for BaTiCu1, BaTiCu2 and BaTiCu3 catalysts. The peak located at the lower temperature, whose intensity increases with the copper content, could correspond to the reduction of copper with a strong electronic interaction with the perovskite, and for hence more easily reducible [32, 61-63], or to copper incorporated into the lattice. It has to be underlined that, though the copper incorporation generates a distortion of the structure creating oxygen vacancies, the coordination of copper in the perovskite structure keeps being higher than that of the CuO [64] and allows its reduction at lower temperature than the CuO used as reference (Figure 4). These H_2-TPR results seem to confirm the conclusions obtained by XPS respect to the relationship between the copper incorporated into the perovskite structure and the copper content. In BaTiCu0.5 catalyst only one

surface copper species, called Cu_S in XPS (Figure 3a), is found and, for the other catalysts, two copper species, surface (Cu_S) and lattice (Cu_L), have been detected.

In addition, it is observed that all copper catalysts show a H_2 consumption at temperatures above 500ºC, probably due to the reduction and/or desorption of the oxygen surface species previously identified by XPS (Figure 3b). In order to prove this hypothesis, a Temperature Programed Desorption experiment in He was carried out for the BaTiCu2 catalyst, which presents a high concentration of surface oxygen species (Table 3). The TCD signal obtained, shown in Figure 5, presents a continuous increase from 350 ºC to 750 ºC that seems to be due to the desorption of oxygen surface groups. Thus, this result seems to confirm that the H_2 consumption observed above 500 ºC in the H_2-TPR experiments corresponds to the reduction of oxygen surface groups. Additionally, a high intensity peak is observed in both H_2-TPR and TPD experiments at temperature higher than 750ºC, which corresponds to the decomposition of $BaCO_3$ (detected by XRD and XPS).

NO_x storage experiments under temperature programmed reaction

As a preliminary activity test, and in order to determine the optimal temperature for isothermal NOx storage experiments, temperature programmed reaction experiments have been carried out. These experiments also give valuable information about the NO to NO_2 oxidation and about the NOx desorption.

Figure 6 presents the NO_x conversion profiles obtained for all catalysts, including the commercial perovskite used as reference (BaTiref). It has to be considered that in Figure 6, the positive values of % NOx conversion indicate that NOx adsorption is taking place, while, the

negative values correspond to a NOx desorption process. Thus, at temperatures lower than 500ºC, approximately, the NOx conversion profiles represent NOx adsorption profiles and, at temperatures higher than 500ºC, these profiles represent NOx desorption profiles. Bare perovskites (BaTi and BaTiref) show a null NOx storage capacity. After copper addition, the NOx adsorption takes place from 200ºC to 450ºC at which the NOx storage capacity maximum is achieved and, subsequently, the NOx desorption is observed between 500ºC and 620ºC with a maximum around 550ºC for all catalysts.

A detailed analysis of the NOx conversion profiles for copper catalysts reveals the presence of two adsorption maxima at around 300 and 450ºC, which seems to indicate that different adsorption sites (related to the oxygen surface species detected by XPS) or different species (barium nitrites and/or barium nitrates) are formed on the catalysts surface [65, 66]. However, only one NOx desorption peak at around 550ºC is displayed, indicating that almost one NOx adsorbed specie is present at the desorption temperature. Note that the NOx conversion (due to NOx adsorption) increases with the copper content but a limit for BaTiCu2 catalyst seems to be achieved (Figure 6).

For NOx adsorption process on alkaline oxides, two routes have been proposed [65, 66]: i) the formation of nitrates on the surface through the adsorption of NO_2 (obtained by oxidation of NO) on the active sites of the catalyst surface (called "nitrate route") and, ii) the adsorption of NO_2 forming nitrites which will be further oxidized to nitrates on the catalyst surface (called "nitrite route"). The two adsorption maxima observed in Figure 6 seem to suggest that, for the $BaTi_{1-x}Cu_xO_3$ catalysts, the two routes coexist during adsorption. The unique desorption maximum seems to reveal that, at the temperature of desorption, the main surface specie is barium nitrate

which is consistent with the two routes proposed. Our first FTIR results [67] confirm this hypothesis, even though a detailed study of the mechanism using FTIR is mandatory.

Additional information is obtained from the analysis of the NO_2 profiles acquired during temperature programmed reaction experiments shown in Figure 7. Before doing the analysis, it has to be mentioned that the feed gas is a NO + O_2 mixture with a NO_2 concentration almost null. The oxidation of NO to NO_2 is thermodynamically favored at low temperature but it is kinetically restricted and, consequently, controls the kinetic of the reaction at low temperature. It is observed that all catalysts tested seem to accelerate the NO oxidation to NO_2 until around 500ºC and, afterwards, the NO_2 percentage decreases due to thermodynamic limitations. For this reason, all NO_2 profiles present a maximum; below the maximum, the NO_2 concentration is kinetically controlled and the catalyst determines the amount of NO_2 emitted, and, above the maximum, the thermodynamic limits the NO_2 production. Bare perovskites (BaTi and BaTiref) are able to accelerate the NO oxidation to NO_2, especially the BaTi perovskite, but, a higher NO to NO_2 oxidation capacity is shown by $BaTi_{1-x}Cu_xO_3$ perovskites.

Note that the NO_2 profiles for $BaTi_{1-x}Cu_xO_3$ catalysts show a minimum for the temperature at which the NOx adsorption profiles achieved the maximum level. Also, it is observed a maximum at a temperature higher than the NO_2 thermodynamic maximum (around 550ºC) which coincides with the temperature for the maximum of NOx desorption observed in Figure 6. From these correlations, it could be deduced that: i) the NOx adsorption depends on the NO_2 generation because NO_2 is more effectively adsorbed than NO and ii) the NO_2 generation depends on the NOx adsorption process as NO_2 is produced upon decomposition of adsorbed NOx species. For bare perovskites (BaTi and BaTiref) this correlation is not observed because these catalysts show a null storage capacity (Figure 6).

From these results it can be inferred that the NO_2 generation pathway is different for bare than for copper perovskites. For copper perovskites, once NO is oxidised to NO_2, a fraction of the NO_2 is adsorbed on the catalyst as barium nitrites and/or barium nitrates and it will be evolved only when the temperature needed for NOx desorption is achieved. As a consequence, the NO_2 produced by copper catalysts should be higher than that shown by NO_2 profiles in Figure 7. For bare perovskites, the absence of NOx adsorption sites (Figure 6) implies that all the NO_2 generated is evolved (Figure 7). Comparing NO_2 profiles of Figure 7, it seems that the NO_2 percentage does not increase with the copper content. However, the NOx storage capacity (Figure 6) is larger for high copper content catalysts (BaTiCu2 and BaTiCu3) and, probably this compensates for the increase of the NO_2 production.

Therefore, it seems that the copper incorporation into the perovskite structure generates active sites for the NO to NO_2 oxidation and for the NOx adsorption. Thus, in agreement with previous conclusions for $SrTi_{1-x}Cu_xO_3$ catalysts [33], copper has to be incorporated into the perovskite structure in order to enhance both the NO to NO_2 oxidation and the NOx storage capacity.

NOx storage experiments under isothermal conditions.

Considering the above discussed results, NOx storage experiments at 420ºC (the temperature at which the maximum NOx conversion is achieved in Figure 6) have been developed using $BaTi_{1-x}Cu_xO_3$ catalysts. Table 4 shows the amount of NOx stored ($\mu mol/g_{catalyst}$), on the catalyst at 420ºC calculated from NOx profiles (see experimental section for details) obtained during the tenth cycle at which the catalysts achieve a reproducible performance. The NOx profiles are compared in Figure 8, where a sharp NOx decrease is observed as soon as the perovskite is put in

contact with the NO + O_2 gas mixture due to the NOx chemisorption on the strongest adsorption sites generated during the reduction of the perovskite (see experimental section for details). Afterwards, the NOx storage decreases very slowly due to the adsorption on less active sites and, then, it drops faster when catalyst surface is being saturated. The data of Table 4 reveal that the NOx storage capacity increases with copper content for BaTiCu0,5, BaTiCu1 and BaTiCu2 whilst, for the highest copper content BaTiCu3 catalyst, the NOx storage capacity almost does not increase, staying close to 300 μmol/$g_{catalyst}$.

The characterization results obtained indicate that the incorporation of copper into the perovskite lattice produces a distortion on the tetragonal structure, the creation of oxygen vacancies and promotes the segregation of some phases (CuO, $BaCO_3$, TiO_2 and Ba_2TiO_4). As a consequence of all these modifications, related with the interaction of copper, barium and oxygen inside the perovskite structure (which depends on the copper content), active sites for both NO to NO_2 oxidation and for NOx storage are created on the copper perovskites. The direct implication of $BaCO_3$, widely reported in the literature as a NOx storage material[4, 68], in the increase of the NOx storage capacity of the copper catalyst seems not to be relevant because barium carbonate is also present in the bare perovskite (BaTi) and this catalyst presents a null NOx storage capacity (Figure 6).

The NOx storage capacity (obtained in similar experimental conditions that the used in this paper) reported in the literature for different catalysts is also compiled in Table 4 and ranges from 33 to 500 μmol/$g_{catalyst}$. The amount of NOx stored at 420 ºC on the BaTiCu2 (the catalyst with the lowest copper content showing the highest NOx storage capacity), which is around 300 μmol/$g_{catalyst}$, is much higher than the corresponding to $SrTi_{1-x}Cu_xO_3$ catalysts due to the presence of Ba instead of Sr [32, 33]. Note that, this value is within the range of values reported for noble

metal/alkali or alkali earth based catalysts at 300ºC or 350ºC. It has to be underlined that the BaTiCu2 perovskite does not incorporate any noble metal, and therefore, could be a cheaper alternative to catalysts based on noble metal. Additionally, as this catalyst works at 420ºC and presents an acceptable NOx storage capacity, it could be used as the component of high-temperature LNT for a lean burn gasoline engine (GDI gasoline direct injection) which needs catalysts working between 400 and 500ºC. For practical application, the NOx Storage Efficiency (NSE), which is the fraction of the NOx fed which is adsorbed during the adsorption step, is the most relevant parameter. Because this parameter is not high enough for the tested $BaTi_{1-x}Cu_xO_3$ catalysts (50% at the highest), we are working in order to optimize the catalysts performance.

IV. Conclusions

From the results above discussed, the following conclusions can be extracted:

- The synthesis method used to prepare $BaTi_{1-x}Cu_xO_3$ catalysts produces perovskites with a tetragonal structure.
- Two copper species with different electronic interaction with the perovskite, and hence with different reducibility, seem to exist on the catalysts surface. The fraction of copper with a stronger electronic interaction with perovskite (or incorporated into the perovskite structure) increases with the copper content. This is the fraction of copper which is reduced at lower temperatures.
- The incorporation of copper into the perovskite lattice generates: i) a distortion of the tetragonal structure, ii) oxygen vacancies on the perovskite structure, iii) active oxygen species on the catalyst surface and, finally, induces the segregation of some species

(CuO, $BaCO_3$, TiO_2 and Ba_2TiO_4). As a consequence of all these modifications, active sites for the NO to NO_2 oxidation and for the NOx adsorption are created on copper perovskite.

- The NOx storage capacity increases with the copper content until a limit is achieved for BaTiCu2 catalyst.
- The BaTiCu2 catalyst presents a NOx storage capacity at 420ºC around 300 $\mu mol/g_{catalyst,}$ which is within the range of values reported for noble metal-based catalyst.
- The $BaTi_{1-x}Cu_xO_3$ catalysts show an acceptable NOx storage capacity and could be used as the component of high-temperature LNT for a lean burn gasoline engine (GDI gasoline direct injection, which needs catalysts working between 400 and 500 ºC), even though the NSE need to be optimized.

V. Acknowledgements.

The authors thank to Spanish Government (MINECO project CTQ2012-030703) and to Generalitat Valenciana (project PROMETEOII/2014/010) for the financial support.

VI. References.

[1] P. Granger, V.I. Parvulescu, Chem. Rev. 111 (2011) 3155-3207.

[2] M.V. Twigg, Catal. Today 163 (2011) 33-41.

[3] Toyota Patent No EP 1,138,890 (2001).

[4] S. Roy, A. Baiker, Chem. Rev. 109 (2009) 4054-4091.

[5] W.S. Epling, L.E. Campbell, A. Yezerets, N.W. Currier, J.E. Parks II, Catal. Rev. 46 (2004) 163-245.

[6] M. Koebel, M. Elsener, M. Kleemann, Catal Today 59 (2000) 335-345.

[7] M.A. Gómez-García, V. Pitchon, A. Kiennemann, Environt. Int. 31 (2005) 445-467.

[8] R. Burch, P.J. Millington, Catal. Today 26 (1995) 185-206.

[9] M. Takeuchi, S. Matsumoto, Top. Catal. 28 (2004) 151-156.

[10] G. Liu, P.X. Gao, Catal. Sci. Tec. 1 (2011) 552-568.

[11] J. Wang, Y. Ji, G. Jacobs, S. Jones, D.J. Kim, M. Crocker, Appl. Catal. B-Environ. 148-149 (2014) 51-61.

[12] D.H. Kim, Y.H. Chin, G.G. Muntean, A. Yezeretz, N.W. Currier, W.S. Epling, H.Y. Chen, H. Hess, C.H.F. Peden, Ind. Eng. Chem. Res. 45 (2006) 8815-8821.

[13] Y. Ji, C. Fisk, V. Easterling, U. Graham, A. Poole, M. Crocker, J.S. Choi, W. Partridge, K. Wilson, Catal Today 151 (2010) 362-375.

[14] Y. Ji, V. Easterling, U. Graham, C. Fisk, M. Crocker, J.S. Choi, Appl. Catal. B-Environ. 103 (2011) 413-427.

[15] D.H. Kim, K. Mudiyanselage, J. Szányi, H. Zhu, J.H. Kwak, C.H.F. Peden, Catal Today 184 (2012) 2-7.

[16] J. Luo, F. Gao, D.H. Kim, C.H.F. Peden, Catal Today 231 (2014) 164-172.

[17] F. Morrison, A. Coats, D. Sinclair, A. West, J Electroceram 6 (2001) 219-232.

[18] G. Arlt, D. Hennings, G. De With, J. Appl. Phys. 58 (1985) 1619-1625.

[19] T. Ishihara, M. Higuchi, T. Takagi, M. Ito, H. Nishiguchi, Y. Takita, J. Mater. Chem. 8 (1998) 2037-2042.

[20] M.T. Buscaglia, V. Buscaglia, M. Viviani, P. Nanni, M. Hanuskova, J. Eur. Ceram. Soc. 20 (2000) 1997-2007.

[21] L.B. Kong, T.S. Zhang, J. Ma, F. Boey, Prog Mater Sci 53 (2008) 207-322.

[22] R.E. Cohen, Nature 358 (1992) 136-138.

[23] M.A. Peña, J.L.G. Fierro, Chem. Rev. 101 (2001) 1981-2017.

[24] V.M. Goldschmidt, Naturwissenschaften 14 (1926) 477-485.

[25] A. Manthiram, J.H. Kim, Y.N. Kim, K.T. Lee, J Electroceram 27 (2011) 93-107.

[26] Z. Li, M. Meng, Y. Zha, F. Dai, T. Hu, Y. Xie, J. Zhang, Appl. Catal. B-Environ. 121-122 (2012) 65-74.

[27] C. Constantinou, W. Li, G. Qi, W.S. Epling, Appl. Catal. B-Environ. 134-135 (2013) 66-74.

[28] X. He, M. Meng, J. He, Z. Zou, X. Li, Z. Li, Z. Jiang, Catal. Commun. 12 (2010) 165-168.

[29] S. Hodjati, K. Vaezzadeh, C. Petit, V. Pitchon, A. Kiennemann, Appl. Catal. B-Environ. 26 (2000) 5-16.

[30] A. Ueda, Y. Yamada, M. Katsuki, T. Kiyobayashi, Q. Xu, N. Kuriyama, Catal. Commun. 11 (2009) 34-37.

[31] C.H. Kim, G. Qi, K. Dahlberg, W. Li, Science 327 (2010) 1624-1627.

[32] F.E. López-Suárez, M. Illán-Gómez, A. Bueno-López, J.A. Anderson, Appl. Catal. B-Environ. 104 (2011) 261-267.

[33] F.E. López-Suarez, S. Parres-Esclapez, A. Bueno-López, M. Illán-Gómez, B. Ura, J. Trawczynski, Appl. Catal. B-Environ. 93 (2009) 82-89.

[34] X.G. Li, Y.H. Dong, H. Xian, W.Y. Hernandez, M. Meng, H.H. Zou, A.J. Ma, T.Y. Zhang, Z. Jiang, N. Tsubaki, P. Vernoux, Energ. Environ. Sci. 4 (2011) 3351-3354.

[35] A.J. Ma, S.Z. Wang, C. Liu, H. Xian, Q. Ding, L. Guo, M. Meng, Y.S. Tan, N. Tsubaki, J. Zhang, L.R. Zheng, X.G. Li, Appl. Catal. B-Environ. 146 (2014) 24-34.

[36] C. Ge, L. Li, H. Xian, H. Yan, M. Meng, X. Li, Fuel Procces Technol. 120 (2014), 1-7.

[37] P. Pechini, Patent No US 3,330,697 (1967).

[38] A. Kareiva, S. Tautkus, R. Rapalaviciute, J.E. Jorgensen, B. Lundtoft, J Mater Sci 34 (1999) 4853-4857..

[39] A. Hardy, J. D'Haen, M. Van Bael, J. Mullens, J.Sol-Gel Sci. Techn. 44 (2007), 65-74.

[40] Y. Narendar, G.L. Messing, Catal Today 35 (1997) 247-268.

[41] S. Brunauer, P.H. Emmett, E. Teller, J. Amer. Chem. Soc. 60 (1938) 309-319.

[42] H. Hayashi, T. Nakamura, T. Ebina, J. Phys. Chem. Solids. 75 (2013) 957.

[43] N. Bouazza, M. Ouzzine, M.A. Lillo-Ródenas, D. Eder, A. Linares-Solano, Appl. Catal. B-Environ. 92 (2009), 377-383.

[44] J.I. Langford, A.J.C. Wilson, J. Appl. Crystallogr. 11 (1978) 102-113.

[45] Y. Hakuta, H. Ura, H. Hayashi, K. Arai, Mater Lett 59 (2005) 1387-1390.

[46] A. Pinczuk, W. Taylor, E. Burstein, I. Lefkowitz, Solid State Commun. 5 (1967) 429-433.

[47] M.S. Chen, Z.X. Shen, S.H. Tang, W.S. Shi, D.F. Cui, Z. H. Chen, J. Phys-Condens. Mat 12 (2000) 7013.

[48] B.D. Begg, K.S. Finnie, E.R. Vance, J Amer Ceram Soc 79 (1996) 2666-2672.

[49] W. Zhang, L. Chen, Y. Tao, W. Zhang, J. Chen, J. Zhang, X, Phys. B-Condens. Mat 406 (2011) 4630-4633.

[50] M. Rossel, H.R. Hoche, H.S. Leipner, D. Voltzke, H.P. Abicht, O. Hollricher, J. Muller, S. Gablenz, Anal. Bioanal. Chem. 380 (2004) 157-162.

[51] F. Wijzen, J. Rocha, A. Esculcas, B. Gilbert, P. Tarte, A. Rulmont, Spectrochim. Acta A 55 (1999) 325-332.

[52] J. Ghijsen, L.H. Tjeng, J. Van Elp, H. Eskes, J. Westerink, G.A. Sawatzky, M.T. Czyzyk, Phys. Rev. B 38 (1988) 11322-11330.

[53] J.P. Espinós, J. Morales, A. Barranco, A. Caballero, J.P. Holgado, A.R. González-Elipe, J Phys Chem B 106 (2002) 6921-6929.

[54] Benoit R., Centre de Recherche sur la Matière Divisée – CNRS. www.lasurface.com (2013).

[55] K. Tabata, Y. Hirano, E. Suzuki, Appl. Catal. A-General 170 (1998) 245-254.

[56] G. Colon, J.A. Navio, R. Monaci, I. Ferino, Phys. Chem. Chem. Phys. 2 (2000) 4453-4459.

[57] H. He, H.X. Dai, C.T. Au, Appl. Catal. B-Environ. 33 (2001) 65-80.

[58] A.E. Nelson, K.H. Schulz, Appl Surf Sci 210 (2003) 206-221.

[59] L. Cadus, N. Merino, B. Barbero, P. Eloy, Appl Surf Sci 253 (2006) 1489-1493.

[60] J.X. Liao, C.R. Yang, Z. Tian, H.G. Yang, L. Jin, J Phys D 39 (2006) 2473-2479.

[61] H. Lei, R.f. Nie, J.h. Fei, Z.y. Hou, J. Zhejiang Univ. Sci. A 13 (2012) 395-406.

[62] L.C. Wang, Y.M. Liu, M. Chen, Y. Cao, H.Y. He, G.S. Wu, W.L. Dai, K.N. Fan, J. Catal. 246 (2007) 193-204.

[63] N. Tien-Thao, H. Alamdari, M.H. Zahedi-Niaki, S. Kaliaguine, Appl. Catal. A-Gen. 311 (2006) 204-212.

[64] J.B. Forsyth, S. Hull, J. Phys. Cond. Matter 3 (1991) 5257-5261.

[65] B. Pereda-Ayo, U. De La Torre, M.P. González-Marcos, J.R. González-Velasco, In press, (2014) http://dx.doi.org/10.1016/j.cattod.2014.03.044.

[66] P. Broqvist, I. Panas, E. Fridell, H. Persson, J Phys Chem B 106 (2002) 137-145.

[67] V. Albaladejo-Fuentes, F.E. López-Suárez, M.S. Sánchez-Adsuar, M.J. Illán-Gómez, Estudio DRIFT del proceso de adsorción de NOx en catalizadores BaTi1-xCuxO3 In: M.A. Centeno, A. Pérez, (Eds.), Catalizadores y reactores estructurados SECAT 2013, (2013) pp. 303-304.

[68] L. Lietti, P. Forzatti, I. Nova, E. Tronconi, J. Catal. 204 (2001) 175-191.

[69] K.S. Kabin, R.L. Muncrief, M.P. Harold, Catal Today 96 (2004) 79-89.

[70] A. Lindholm, N.W. Currier, E. Fridell, A. Yezerets, L. Olsson, Appl. Catal. B-Environ. 75 (2007) 78-87.

[71] H.Y. Huang, R.Q. Long, R.T. Yang, Energ. Fuel 15 (2001) 205-213.

Table 1. Molecular composition, BET surface, copper content, molar % of Cu reduced during H_2-TPR, average crystal size, cell parameters, FWHM (200)/(111) ratio and crystalline structure for the $BaTi_{1-x}Cu_xO_3$ catalysts.

Catalyst	Molecular composition	BET Surface area (m^2/g)	Nominal Cu (wt %)	ICP Cu (wt %)	Cu reduced during H_2-TPR (molar %)	Average crystal size (nm)	a (Å)	c (Å)	FWHM (200)/(111)	Crystalline stucture
BaTiref	$BaTiO_3$	-	-		-	29	4.011	4.005	1.48	T
BaTi	$BaTiO_3$	9	-		-	29	4.011	4.007	1.27	T
BaTiCu0,5	$BaTi_{0.95}Cu_{0.05}O_3$	13	1.4	1.4	63	35	4.007	4.009	1.31	T
BaTiCu1	$BaTi_{0.9}Cu_{0.1}O_3$	16	2.7	2.7	88	38	4.008	4.009	1.44	T
BaTiCu2	$BaTi_{0.8}Cu_{0.2}O_3$	21	5.4	5.4	93	38	4.008	4.008	1.44	T
BaTiCu3	$BaTi_{0.7}Cu_{0.3}O_3$	26	8.0	8.0	85	38	4.008	4.009	1.55	T

Table 2. XPS Characterization of the copper species for the $BaTi_{1-x}Cu_xO_3$ catalysts

Catalyst	Cu 2p3/2 level				Cu/ [Ba+Ti+Cu] (XPS)	Cu/ [Ba+Ti+Cu] (nominal)	Cu+Ti/ Ba
	Cu_s (eV)	Area	Cu_L (eV)	Area			
BaTiref	-		-		-		0.977
BaTi	-		-		-		0.720
BaTiCu0,5	933.8	100 %	-		0.025	0.025	0.450
BaTiCu1	933.5	57 %	935.2	43 %	0.051	0.05	0.555
BaTiCu2	933.5	55 %	935.2	45 %	0.064	0.1	0.491
BaTiCu3	933.7	47 %	935.6	53 %	0.144	0.15	0.366

Table 3. XPS Characterization of the oxygen species for the $BaTi_{1-x}Cu_xO_3$ catalysts.

Catalyst	O 1s level						O_L/ (Ba+Ti+Cu)
	O_L (eV)	Area	O* (eV)	Area	H_2O (eV)	Area	
BaTiref	529.8	63 %	532.0 ()	37%	-		2.051
BaTi	529.9	65 %	532.0	35 %	-		1.78
BaTiCu0,5	529.7	43 %	531.9	53 %	533.9	4 %	1.34
BaTiCu1	529.9	50 %	532.0	45 %	534.0	5 %	1.5
BaTiCu2	529.9	44 %	532.0	51 %	534.0	4 %	1.46
BaTiCu3	530.0	39 %	532.1	57 %	534.1	5 %	1.24

Table 4. Comparison of the NOx storage capacity data.

Catalyst	NOx storage capacity (µmol/g)	Experiment conditions		Ref.
		Temperature (ºC)	Lean cycle time (s)	
BaTiCu0,5	130	420	300	
BaTiCu1	230	420	300	
BaTiCu2	292	420	300	
BaTiCu3	300	420	300	
$SrTi_{0.89}Cu_{0.11}O_3$*	33	300	300	[32]
1% Pt/20% BaO/Al_2O_3	150	350	120	[68]
2.2% Pt/16.3% BaO/Al_2O_3	400	350	240	[69]
2.2% Pt/16.3% BaO/Al_2O_3	500	350	480	[69]
2.9% Pt/20.8% BaO/Al_2O_3	240	300	240	[70]
1% Pt/5% CaO/Al_2O_3	180	300	450	[71]
1% Rh/5% CaO/Al_2O_3	280	300	450	[71]
1% Pd/5% CaO/Al_2O_3	97	300	450	[71]

**Calculated from the first 300 seconds of the experiment in order to compare with our experiment conditions time*

Figure 1a. XRD diffractograms of the $BaTi_{1-x}Cu_xO_3$ catalysts. ● $BaTiO_3$, ▼ TiO_2, ▲ CuO, ■ Ba_2TiO_4, ♦ $BaCO_3$.

Figure 1b. Magnification of the XRD diffractograms to identify the (110), (111) and (200) perovskite peaks.

Figure 2. Raman spectra of the $BaTi_{1-x}Cu_xO_3$ catalysts.

Figure 3. a) Cu $2p^{3/2}$ XPS transition of the $BaTi_{1-x}Cu_xO_3$ catalysts and b) O1s XPS transition of the $BaTi_{1-x}Cu_xO_3$ catalysts.

Figure 4. H_2-TPR profiles of the $BaTi_{1-x}Cu_xO_3$ catalysts.

Figure 5. TPD profile of the $BaTi_{0.8}Cu_{0.2}O_3$ catalyst.

Figure 6. NOx conversion profiles of the $BaTi_{1-x}Cu_xO_3$ catalysts during temperature programmed reaction. (Experiments were carried out under a gas flow (500 ml/min) containing 500 ppm NO_x, 5 % O_2 in N_2 balance.)

Figure 7. NO_2 generation profiles of the $BaTi_{1-x}Cu_xO_3$ catalysts during temperature programmed reaction. (Experiments were carried out under a gas flow (500 ml/min) containing 500 ppm NO_x, 5 % O_2 in N_2 balance.)

Figure 8. NOx adsorption profiles of the $BaTi_{1-x}Cu_xO_3$ catalysts during the tenth storage-reduction cycle at 420 ºC. (Experiments were carried out using 500 ppm NO_x + 5% O_2 in N_2 balance for 5 minutes, as lean conditions and 10% H_2 in N_2 balance for 2 minutes, as rich conditions.)

Fig.1

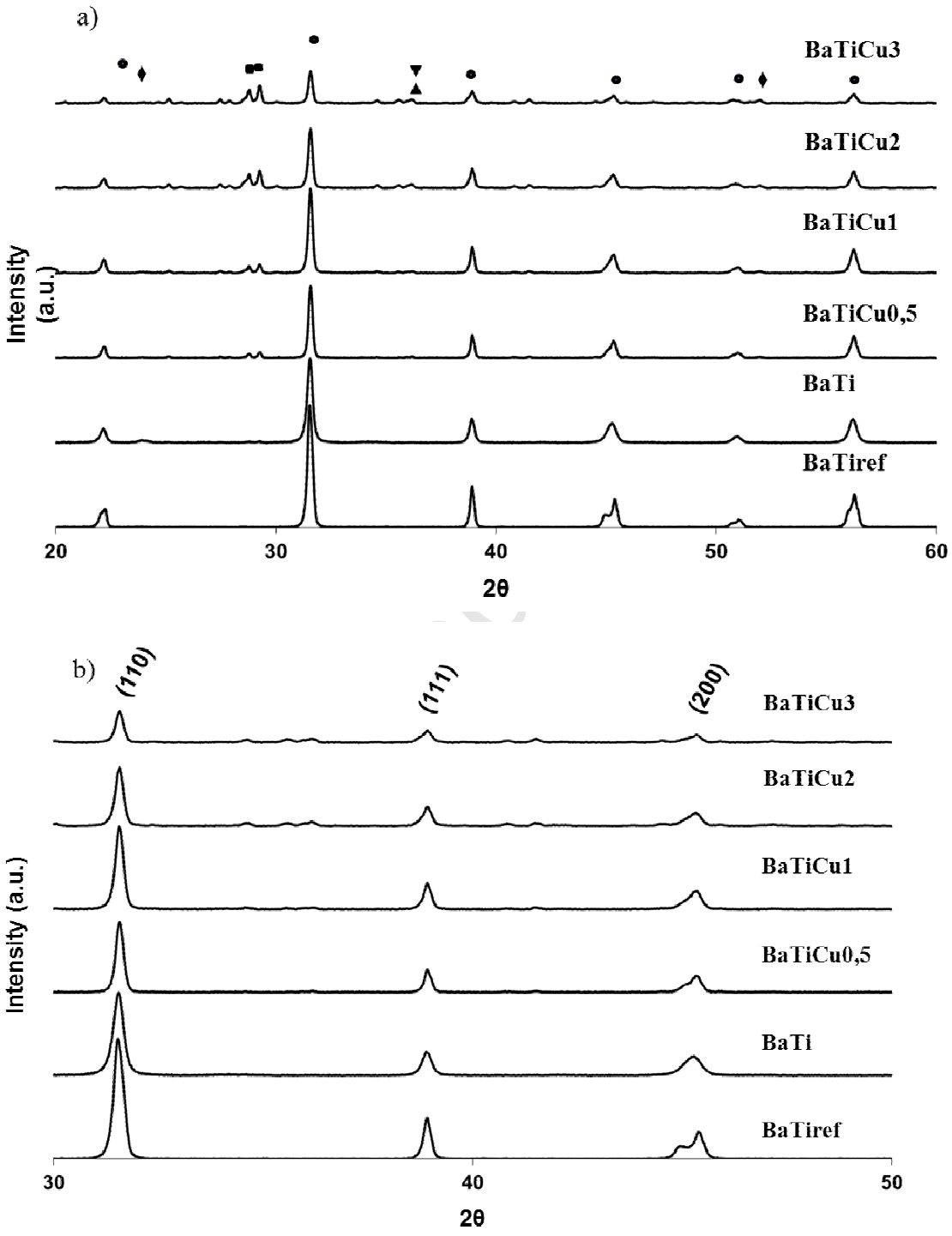

Fig.2

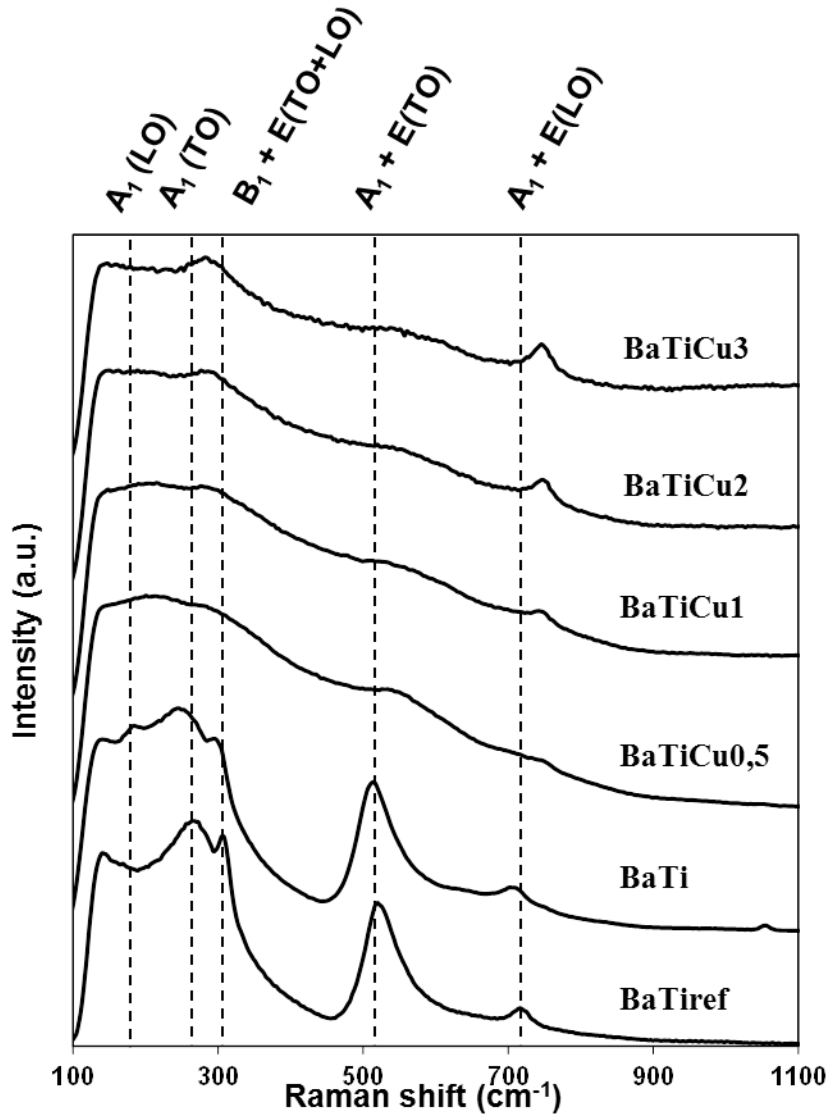

Fig.3

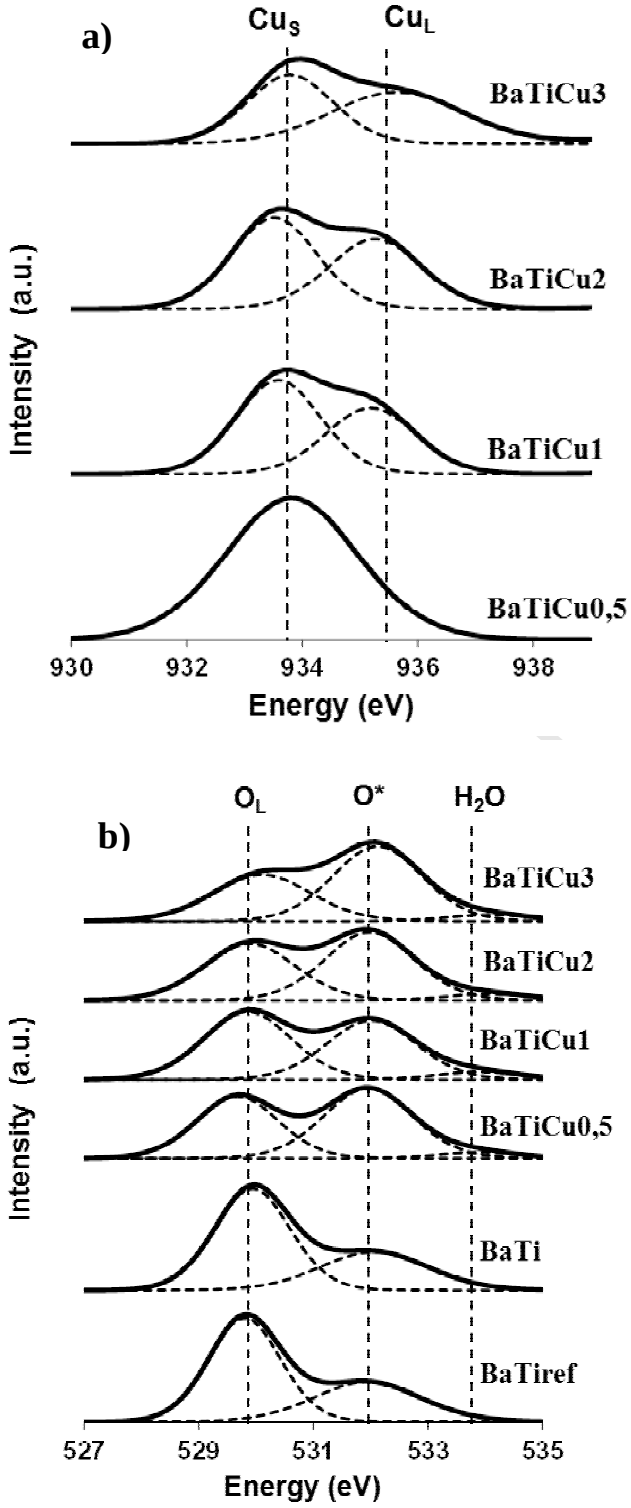

Fig.4

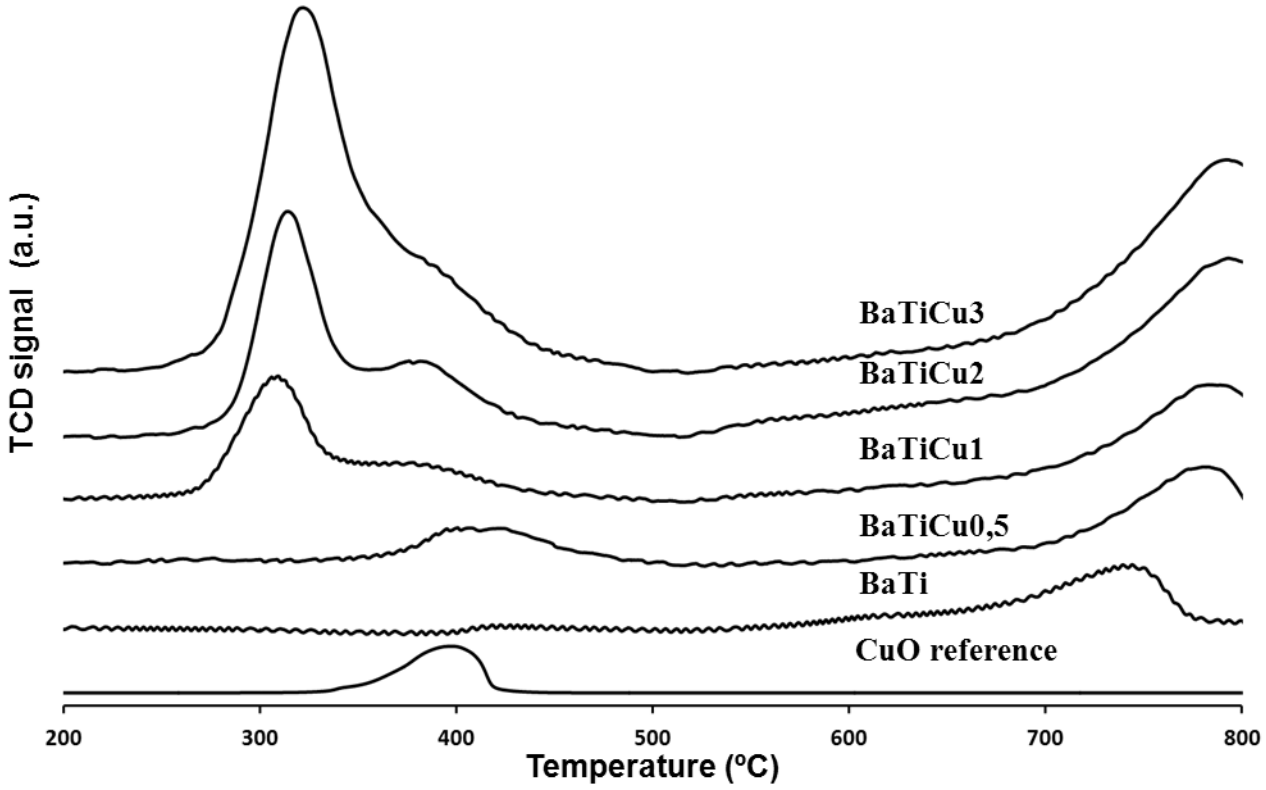

Fig.5

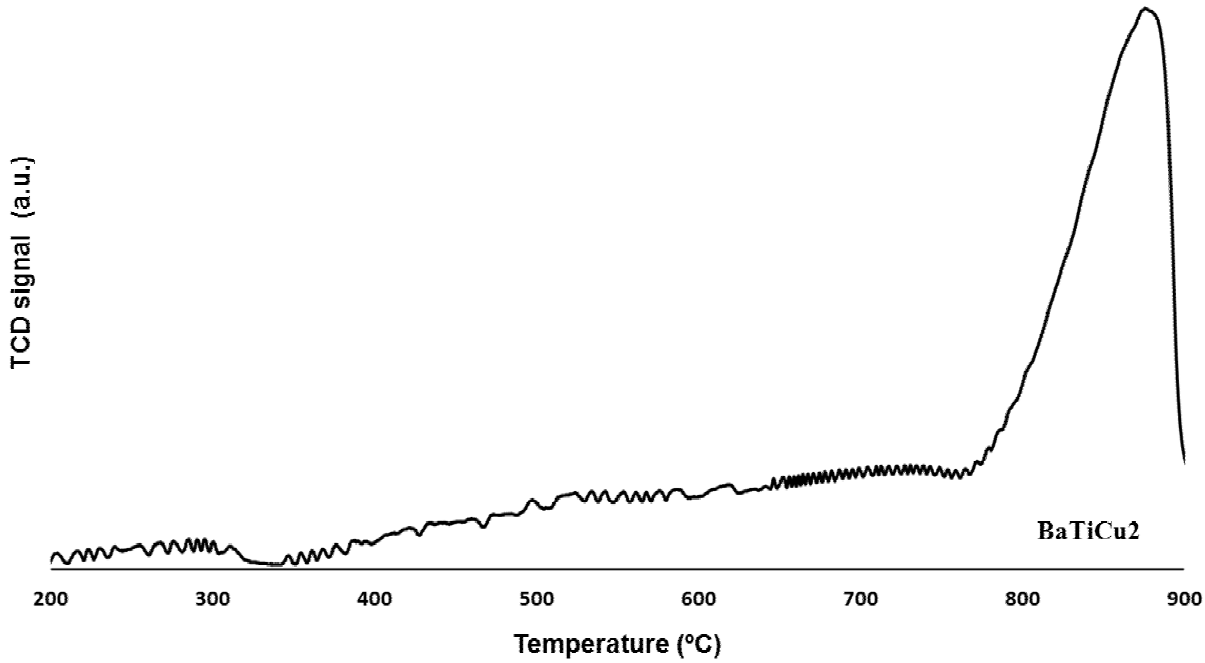

Fig.6

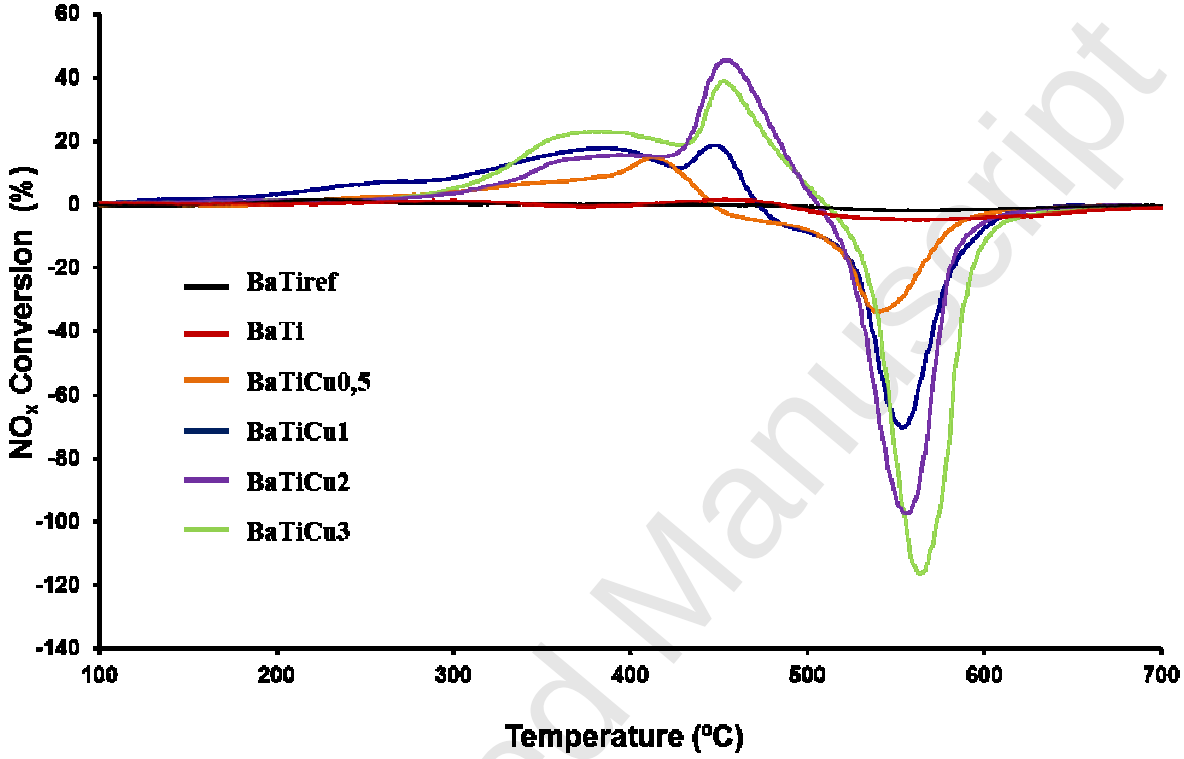

Fig.7

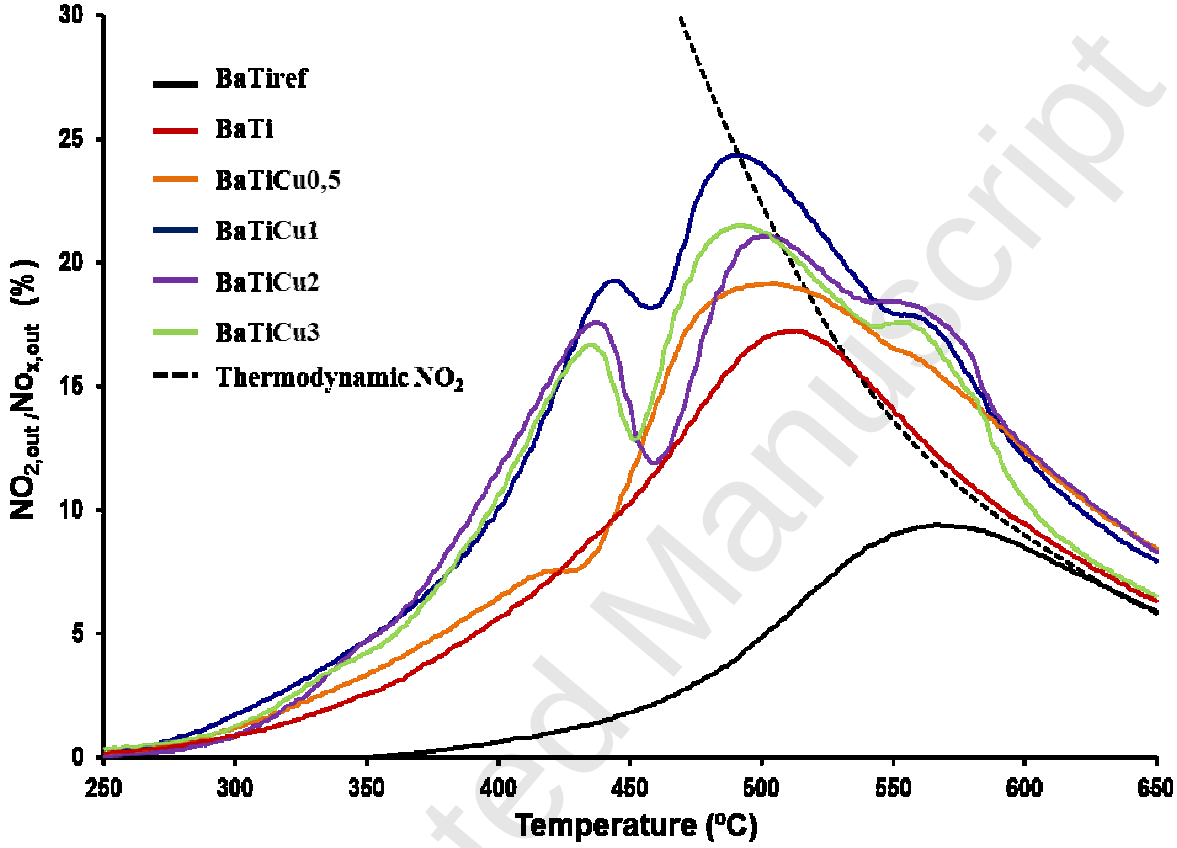

Fig.8